Ceramics-Silikáty 67 (2), 159-166 (2023)
www.ceramics-silikaty.cz doi: 10.13168/cs.2023.0013

SYNTHESIS OF HIGH BELITE SULFOALUMINATE CEMENT CONTAINING MAGNESIA-ALUMINA SPINEL WITH SOLID WASTE

LIANG YU*, JIE ZHANG**, ZENGYAO WANG*, JINGHUA YAN*, #SHOUDE WANG*, #PIQI ZHAO*, XIN CHENG*

*Shandong Provincial Key Laboratory of Preparation and Measurement of Building Materials, University of Jinan, Jinan 250022, China
**Shandong Jianke Building Materials Co. Ltd, Ji'nan

#E-mail: 13589047192@163.com

Submitted February 20, 2023; accepted March 24, 2023

Keywords: Belite sulfoaluminate cement, High magnesium limestone, Solid waste, Phase formation

A high belite sulfoaluminate cement clinker containing a magnesia-alumina spinel was prepared using industrial solid waste and high-magnesium limestone. The preparation procedure and the influence of the trace elements on the clinker were specifically investigated. This study reveals the mechanism of the clinker formation. The appropriate firing temperature of the clinker and holding time were determined to be 1300 °C and 60 – 90 min, respectively. The presence of MgO and SO_3 displayed a positive effect on the clinker formation at high temperatures. In addition, the excessive MgO in the raw material was solidified to create the stable inertia mineral $MgAl_2O_4$, which eliminated the delaying expansion hazard of MgO.

INTRODUCTION

Gold and aluminium industrial solid waste refers to various solid waste slag, dust, and other waste (such as gold tailings, red mud, non-ferrous metal waste slag, desulfurised gypsum, etc.) produced in the process of gold and aluminium production. For its large reserves and availability, it has attracted the attention of many experts and scholars [1, 2]. Gold and aluminium industrial solid waste still has some usable value for other industries. For example, valuable materials in the waste can be recovered for reuse. Gold tailings contain a certain amount of gold, silver, and other elements. These elements can be recovered by a non-ammonia thiosulfate system [3]. Some researchers recovered iron from Bayer red mud using different processes. Moreover, the recovery rates are all very high [4, 5]. Solid waste can also be used as mine fill [6] or road fill [7]. In addition, the solid waste is basically of a similar chemical composition to traditional building materials; therefore, it can replace traditional raw materials for the preparation of cement and other building materials [8–10].

MgO in a cement clinker is generally present as free MgO. A little amount of MgO can promote the formation of the clinker mineral phase and crystalline transformation [11], and contribute to the sintering of the clinker [12]. However, too much MgO will crystallise to form free periclase, and its hydration will cause volume expansion, resulting in poor cement stability [13]. It is required that the MgO content of the limestone used in the production of cement clinkers should be less than 3 %. As a result, limestone with a high Mg content is not effectively used, resulting in a waste of resources [14].

High-belite cement is a low-calcium, low-carbon cementitious material with belite (β-C_2S) as the dominant mineral. It has the advantages of a low energy consumption for its preparation, low heat for hydration, and high mid to late strength. However, the slow hydration of β-C_2S leads to insignificant early strength [15, 16]. To improve its early strength, some researchers introduced calcium sulfoaluminate ($C_4A_3\$$) into this system and created a high-belite sulfoaluminate cement (HB$AC) [17, 18]. Moreover, the availability of raw materials is a prerequisite for its large-scale production. Many researchers started to study the preparation of HB$AC using industrial solid waste, such as fly ash, bauxite, phosphogypsum, and basic oxygen furnace (BOF) slag [18–20]. Extensive studies have proven the feasibility of applying various industrial solid waste to produce HB$AC [21].

In this paper, HB$AC was prepared from a typical gold and aluminium industrial solid waste (mainly including gold tailings, red mud, and desulfurised gypsum) in Shandong Province, China, supplemented with high-magnesium limestone and low-grade bauxite. The thermogravimetric analysis (TG), micro-quotient thermogravimetric analysis (TGA), X-ray diffraction (XRD), and variation of free calcium oxide (f-CaO) content of the samples were used to determine the calcination regimes of the gold-aluminium industrial solid waste-based clinker of HB$AC containing magnesium-aluminium spinel ($MgAl_2O_4$) and the mechanism of the clinker formation.

Table 1. The main compositions of the raw materials.

Raw materials	Composition (wt. %)								
	LOI	SiO_2	Al_2O_3	CaO	SO_3	Fe_2O_3	K_2O	Na_2O	MgO
GT	3.16	64.07	17.52	2.58	1.16	2.54	4.55	2.55	1.18
RM	11.23	15.61	22.37	3.33	0.31	26.62	0.07	12.89	0.15
HML	41.72	4.44	1.21	47.52	0.08	0.57	0.37	–	3.98
DG	21.87	2.11	0.80	32.41	41.21	0.34	0.14	0.17	0.95
BX	14.38	7.49	58.96	8.11	2.42	1.83	0.88	0.10	0.29

EXPERIMENTAL

Raw materials

The used raw materials were gold tailings (GT), red mud (RM), desulfurised gypsum (DG), high-magnesium limestone (HML), and low-grade bauxite (BX). The GT was from a landfill in Zhaoyuan, Shandong Province. The RM was from Shandong Shanlv New Material Environment Co., Ltd. The HML and BX were from Zibo Yunhe Color Cement Co., Ltd. The DG was from Inner Mongolia Energy Power Generation Investment Co., Ltd. The main chemical compositions analysed by X-ray fluorescence (XRF) are presented in Table 1.

Table 2. Chemical composition of the raw material mineral phase.

Corresponding chemical composition (wt. %)					
CaO	SiO_2	Al_2O_3	SO_3	Fe_2O_3	MgO
48.04	16.09	18.12	6.95	3.04	3.80

Design principles

The solid waste-based high belite sulfoaluminate cement (SWB$C) clinker composition was ideally considered to contain only three minerals: $C_4A_3\$$, C_2S, and C_4AF. All the iron phases participated in the reaction to form C_4AF, and the remaining Al_2O_3 and CaO were involved in the formation of $C_4A_3\$$ and C_2S, respectively.

The relationship between the chemical composition and the mineral phase is shown in Equations (1) ~ (5).

$$\omega(CaO) = 0.6512\,\omega(C_2S) + 0.3672\,\omega(C_4A_3\$) + 0.4609\,\omega(C_4AF) \quad (1)$$

$$\omega(SiO_2) = 0.3488\,\omega(C_2S) \quad (2)$$

$$\omega(Al_2O_3) = 0.5012\,\omega(C_4A_3\$) + 0.2099\,\omega(C_4AF) \quad (3)$$

$$\omega(Fe_2O_3) = 0.3292\,\omega(C_4AF) \quad (4)$$

$$\omega(SO_3) = 0.1312\,\omega(C_4A_3\$) \text{ [22]} \quad (5)$$

Based on the principle that the sum of the corresponding dry base oxides of each raw material is equal to the chemical composition of the clinker, the ingredient composition of the raw meal is obtained by solving the matrix to calculate the mass fraction accounted for by each raw material (see Table 2).

Synthesis of the clinkers

According to the dosing scheme, the raw materials were measured separately using an electronic balance and mixed uniformly for 120 min using a QM-4L planetary ball mill with a speed of 200 rpm followed by oven drying overnight at 90 °C. Then, the mixed ground powder mixed with 5 % water was pressed into a disk mould (ø 60 mm × 10 mm) with a pressure of 20 MPa followed by drying the acquired specimen. The raw material was raised from room temperature to 1000 °C in a high-temperature muffle furnace at a heating rate of 5 °C·min^{-1}. Later, the temperature was increased from 1000 °C to a designed temperature at a rate of 3 °C·min^{-1} and then held at that temperature for a certain amount of time. Immediately after the sintering process, the clinkers were allowed to cool down rapidly to room temperature. Finally, the cooled clinkers were ground to ensure that they passed through a 200-mesh sieve.

Testing methods

The phase compositions and hydration products were determined by XRD (D8-ADVANCE) with Cu Kα (λ = 1.54 Å) radiation at 40 kV and 40 mA at a scanning speed of 2 °·min^{-1} over the 2θ range of 5° ~ 70°. TG-DTG was conducted (TGA/DSCI, CH) to measure the mass loss at a heating rate of 10 °C·min^{-1}. An XRF spectrometer (1800 type, Shimadzu Co., Japan) was employed to characterise the chemical composition of the raw materials. The content of *f*-CaO in the clinker was determined by the ethylene glycol-anhydrous ethanol test. The key groups of the clinker minerals were confirmed by a Nicolet iS10 Fourier infrared spectrometer.

RESULTS AND DISCUSSION

Clinker formation analysis

To clarify the physicochemical reactions that occur in the clinker at different firing temperatures, the uniformly mixed raw material was placed into a 7 mm alumina crucible and elevated from 30 °C to 1350 °C at

a heating rate of 10 °C·min^{-1}. Figure 1 depicts the thermal weight loss curves (TG, dummy curve) and micro-quotient thermal weight loss curves (DTG, solid curve) as a result of the TG and DTG for the clinker firing process.

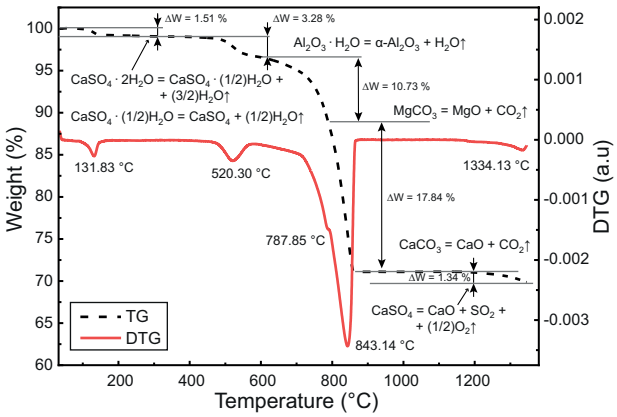

Figure 1. TG-DTG analysis of the firing process.

The TG curve clearly shows four mass losses in the temperature range of 30-1350 °C, while the DTG curve shows five characteristic weight loss peaks. The TG curve shows that the mass loss starts at 99.97 °C, indicating that the detachment of the physical adsorption of water from evaporation already started at this temperature. The weight loss at 131.53 °C indicates that $CaSO_4 \cdot 2H_2O$ in the desulfurised gypsum undergoes dehydration reactions (Equations 6 and 7) that obviously caused the weight loss.

$$CaSO_4 \cdot 2H_2O = CaSO_4 \cdot (1/2)\,H_2O + (3/2)\,H_2O\uparrow \quad (6)$$

$$CaSO_4 \cdot (1/2)\,H_2O = CaSO_4 + (1/2)\,H_2O\uparrow \quad (7)$$

The TG curve shows a second stage of weight loss at 451.78 °C, while the DTG curve also show the weight loss was completed at 520.30 °C, which is caused by the diaspore in the BX [23], which is shown in Equation 8.

$$Al_2O_3 \cdot H_2O = Al_2O_3 + H_2O\uparrow \quad (8)$$

At 614.45 °C, the TG curve shows a large mass loss, because the carbonate minerals in the raw materials start to decompose. The DTG curve has a small peak at 787.85 °C, which should be the decomposition reaction of dolomite ($CaMg(CO_3)_2$) in the high-Mg limestone at this temperature [22]. At 843.14 °C, the rate of CO_2 emissions is at its maximum. At 860.72 °C, the weight loss curve tended to be flat, which indicates that the decomposition of the carbonate minerals is almost complete. Therefore, the reactions of Equations 9 ~ 11 or Equations 11 and 12 are likely to occur in this temperature interval.

$$CaMg\,(CO_3)_2 = MgCO_3 + CaCO_3 \quad (9)$$

$$MgCO_3 = MgO + CO_2\uparrow \quad (10)$$

$$CaCO_3 = CaO + CO_2\uparrow \quad (11)$$

$$CaMg\,(CO_3)_2 = CaO + MgO + 2\,CO_2\uparrow \quad (12)$$

The TG curve showed the fourth stage of weight loss started at 1204.71 °C, and the mass loss increased as the temperature increased and peaked at 1334.13 °C, indicating that the sulfur-containing minerals started to decompose at 1204.71 °C. For example, $CaSO_4$ [24] see Equation 13.

$$CaSO_4 = CaO + SO_2\uparrow + (1/2)\,O_2\uparrow \quad (13)$$

It can be seen that in the process of the clinker mineral generation, the decomposition of $CaSO_4$ might cause a negative impact on the reduction of $C_4A_3\$$, so the amount of gypsum admixture needs to be appropriately increased in the batching calculation to compensate for the loss. It can be found that the decomposition temperature of the solid-phase reaction of each mineral is lower than that in the conventional belite sulfoaluminate cement clinker, which could be attributed to ions-impurities in the solid waste. The impurities might change the corresponding reaction potential and reduce the reaction temperature [25].

Combined with the TG-DTG curve, it can be concluded that the clinker should be fired in the temperature range between 860.72 °C and 1334.13 °C, i.e., from the temperature at which the decomposition of carbonate minerals is completed to the temperature at which the sulfur-containing minerals are substantially reduced [26].

Effect of the firing temperature

Understanding the effect of the firing regime on the formation and decomposition of the clinker mineral phase can provide the basis for further studies on the preparation of SWB$C in the future [27].

Mineral phase generation analysis

With the increase in calcination temperature, $C_4A_3\$$ will decompose and the amount of liquid phase in the clinker will increase, i.e., melting, which means that the calcination temperature is crucial for the firing of the clinker mineral phase. To determine the optimal firing temperatures, the mineral compositions of the cement clinker burnt at different calcination temperatures above 1100 °C were analysed by X-ray diffraction, and the results are demonstrated in Figure 2.

Figure 2 shows that the C_2S diffraction peak intensity does not change significantly during clinker calcination, whereas the $C_4A_3\$$ diffraction peak intensity increases with the increasing temperature. When the calcination temperature was increased from 1100 °C to 1250 °C, the diffraction peak intensities of calcium-aluminium

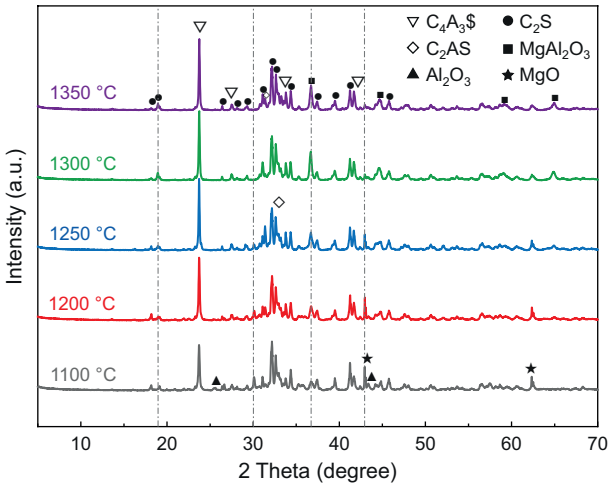

Figure 2. XRD patterns of the clinker at different firing temperatures.

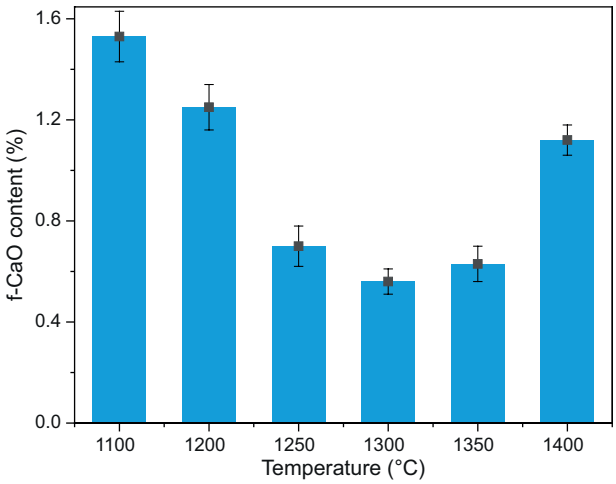

Figure 3. Variation in the *f*-CaO content in the clinker at different temperatures.

xanthite ($2CaO–Al_2O_3–SiO_2$, C_2AS) and $MgAl_2O_4$ enhanced significantly, while the diffraction peaks of MgO and Al_2O_3 weakened significantly. When the temperature rises to 1300 °C, the diffraction peaks of C_2AS, MgO, and Al_2O_3 are not obvious, and the diffraction peaks for $C_4A_3\$$, C_2S, and $MgAl_2O_4$ have a full peak shape. This indicates that the reaction of C_2AS, MgO, and Al_2O_3 is almost complete at this temperature, and the corresponding cement clinker minerals are well developed and formed in abundance. The solid phase reactions are described by Equations 14 ~ 16.

$$2\,CaO + Al_2O_3 + SiO_2 = 2\,CaO \cdot Al_2O_3 \cdot SiO_2 \quad (14)$$

$$3\,CaO + 3\,(2\,CaO \cdot Al_2O_3 \cdot SiO_2) + CaSO_4 = \\ = 3\,CaO \cdot 3\,Al_2O_3 \cdot CaSO_4 + 3\,(2\,CaO \cdot SiO_2) \quad (15)$$

$$MgO + Al_2O_3 = MgAl_2O_4 \quad (16)$$

When the temperature reaches 1350 °C, faint C_2AS peaks appear again in the XRD pattern. This is produced by the solid-phase reaction with C_2S or SiO_2 following the decomposition of $C_4A_3\$$, so the clinker should be fired between 1250 °C and 1350 °C.

f-CaO determination

The *f*-CaO content in the cement clinker was measured to obtain the optimum firing temperature interval because it reflects the ease of firing the cement clinker. The results are shown in Figure 3.

The *f*-CaO concentration in the clinker decreases and subsequently increases when the calcination temperature of the clinker rises, as shown in Figure 3. When the calcination temperature increase from 1100 °C to 1300 °C, the *f*-CaO content decreases from 1.53 % to 0.56 %. The *f*-CaO content in the clinker increased when the calcination temperature exceeded 1300 °C. The increased *f*-CaO was possibly produced by the decomposition of $CaSO_4$ or $C_4A_3\$$ in the clinker. At the calcination temperature of 1300 °C, the *f*-CaO content drops to a relative minimum, which indicates that the reaction of the active mineral phase in the clinker is basically complete, i.e., the cement clinker is successfully fired at 1300 °C. This result is consistent with the results analysed in Figure 2.

FT-IR analysis

Each active mineral phase has a specific wavelength position in the infrared absorption band, and the intensity of the absorption band can indicate the mineral phase's crystallographic development to some extent. The infrared absorption spectra of the clinker at different firing temperatures are displayed in Figure 4.

Figure 4 exhibits that the positions of the peaks of the clinker fired at different temperatures are similar. For example, the IR patterns of clinker samples fired at 1100 °C were analysed for functional groups: The absorption peaks at wave numbers around 1195.71 cm^{-1}, 1112.78 cm^{-1}, 876.64 cm^{-1}, 692.35 cm^{-1}, 644.14 cm^{-1},

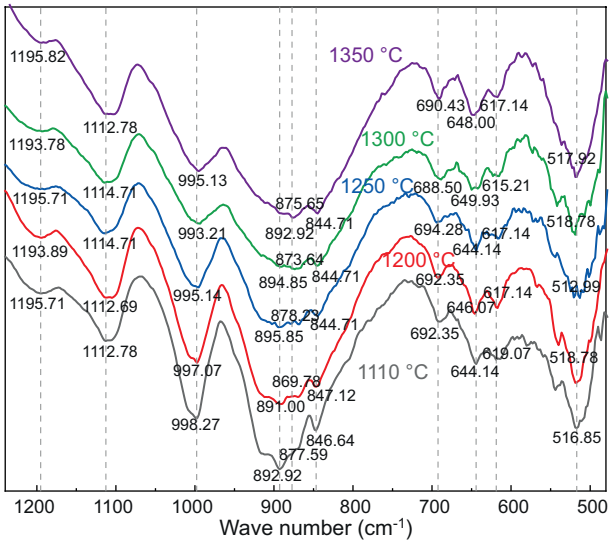

Figure 4. Infrared absorption spectra of the clinker at different firing temperatures.

and 619.07 cm^{-1} are from the vibrations of the functional groups of $C_4A_3\$$. The absorption peaks around 1195.71 cm^{-1} and 1112.78 cm^{-1} are due to the asymmetric stretching vibration of the $[SO_4]$ tetrahedra in $C_4A_3\$$. The peak at 876.64 cm^{-1} is the absorption peak of the asymmetric stretching vibration of $[AlO_4]$. The vibrational coupling of $[AlO_4]$ tetrahedra and $[SO_4]$ tetrahedra causes the appearance of three absorption peaks between 600 cm^{-1} and 700 cm^{-1}. The absorption peaks at wave numbers around 998.27 cm^{-1}, 892.92 cm^{-1}, 846.64 cm^{-1}, and 516.85 cm^{-1} are from the vibrations of the C_2S functional group. The C_2S minerals are made up of isolated $[SiO_4]$ tetrahedra attached to the Ca atoms. The absorption peaks at 998.27 cm^{-1}, 892.92 cm^{-1} and 846.64 cm^{-1} are due to the asymmetric stretching vibrations of the $[SiO_4]$ tetrahedra and the absorption band at 516.85 cm^{-1} is a result of the bending vibration of the $[SiO_4]$ tetrahedra.

The absorption peak positions of $C_4A_3\$$ and C_2S minerals in the fired clinker differ from those in the pure mineral phase. It indicates that the two minerals in the clinker are solid solutions formed by reliable solutions of some other mineral ions. This will produce lattice distortion and improve the hydration activity of the cement clinker [25].

Effect of the holding time

Because the solid-phase reactions required to produce the target minerals need a specific amount of energy, maintaining the clinker at a firing temperature for a specific period is essential for the production and growth of each mineral in the clinker. The target minerals would probably not be generated fully if the holding duration is too brief and the energy input is insufficient, which negatively affects the performance of the cement clinker. If the holding period is too long, too much energy is provided, which might cause excessive crystallisation or mineral decomposition [28]. Thus, choosing the proper holding time is crucial for firing clinker.

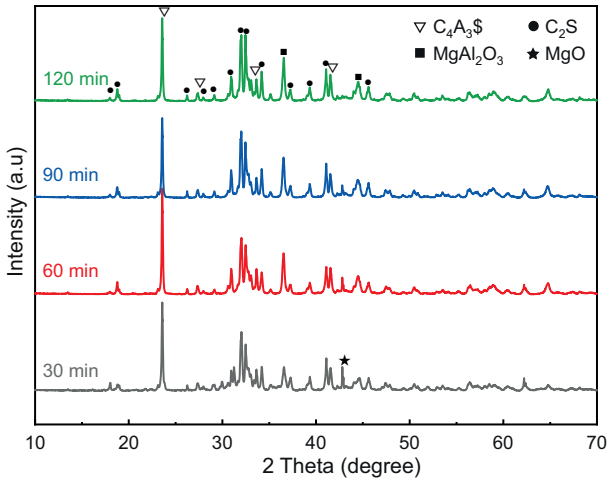

Figure 5. XRD patterns of the clinker at different holding times.

XRD analysis

To determine the optimal holding time for clinker fired at 1300 °C, raw material flakes of the same ratio were heated to 1300 °C for 30 min, 60 min, 90 min, and 120 min in the muffle furnace. The prepared specimens were then subjected to XRD tests, and the results are shown in Figure 5.

It is evident from Figure 5 that the main minerals of the clinker are C_2S, $C_4A_3\$$, and $MgAl_2O_4$. The peak intensity of C_2S grows significantly with the extension of the holding time, which indicates that the C_2S grains grow with the extension of the holding time. As the holding time was extended from 30 min to 90 min, the diffraction peak of MgO decreased and the diffraction peak of $MgAl_2O_4$ increased, which indicates that $MgAl_2O_4$ was continuously generated with the extension of the holding time. The peak intensity of the $C_4A_3\$$ diffraction peak increased and then decreased as the holding time increased. The highest peak intensity was observed at 60 min of holding time, which means that the maximum amount of $C_4A_3\$$ is produced at a holding time of 60 min. However, with the extension of the holding time, the decomposition of $CaSO_4$ hindered the continuation of the solid-phase reaction to produce $C_4A_3\$$ and part of $C_4A_3\$$ decomposed. As a result, the $C_4A_3\$$ content decreases.

f-CaO determination

Figure 6 depicts the variation in the *f*-CaO content in the fired clinker at different holding times.

Figure 6 reveals that the *f*-CaO content in the clinker tends to decrease with the increase in the holding time. During calcination, MgO generally replaced CaO in the target minerals, which led to a decrease in the *f*-CaO content. After holding for 90 min, the MgO in clinker was converted into $MgAl_2O_4$, leading to a significant decrease in the *f*-CaO. The extension of the holding time

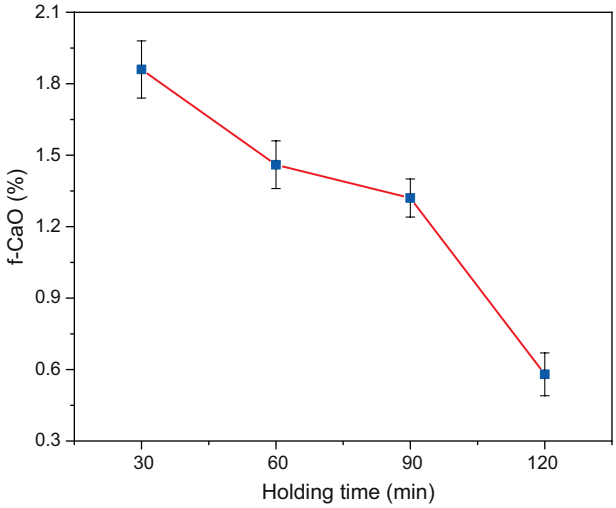

Figure 6. Variation in the *f*-CaO content in the clinker at different holding times.

is beneficial to the formation and growth of the active mineral phase in the clinker. The conclusion is consistent with the results from Figure 5.

Effect of trace elements

Trace elements have a significant influence on cement firing: they can increase the amount of liquid phase during cement firing and also participate in the formation of the main minerals in the cement clinker [29].

Effect of MgO on the clinker mineral phase

The MgO content has a significant impact on the clinker quality. Not only does it affect the production of the stable inertia mineral $MgAl_2O_4$, but also any excessive addition can cause volume expansion [30]. The prepared clinker was ground and tested by XRD, and the results are presented in Figure 7.

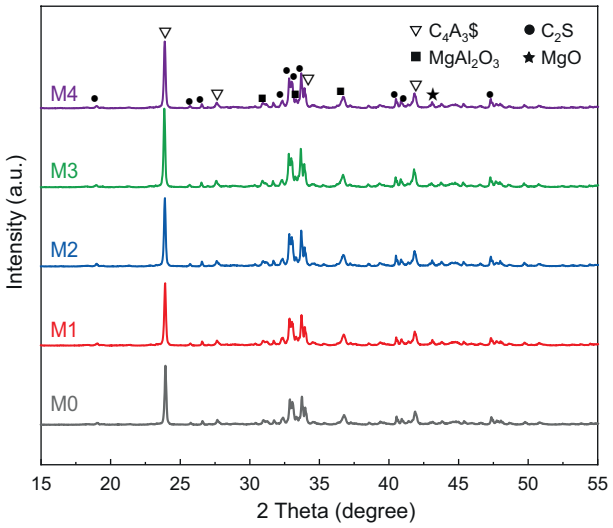

Figure 7. XRD patterns of the clinker with different amounts of MgO.

Figure 7 illustrates that the peak intensities of $C_4A_3\$$ and $MgAl_2O_4$ rise with the MgO addition, which means that the presence of MgO is beneficial to the formation of $C_4A_3\$$ and $MgAl_2O_4$. The additions of MgO were effectively fixed even when the MgO additions reached 5.3 %, the diffraction peaks of MgO did not obviously appear in Figure 7.

Effect of SO_3 on the clinker mineral phase

It was noticed in Figure 1 that the clinker started to show a significant mass loss at 1204.71 °C of calcination on account of the decomposition of $CaSO_4$. As a result, an additional appropriate amount of SO_3 must be added to the system to meet the designed $C_4A_3\$$ content. The prepared clinker was tested by XRD, and the results are presented in Figure 8.

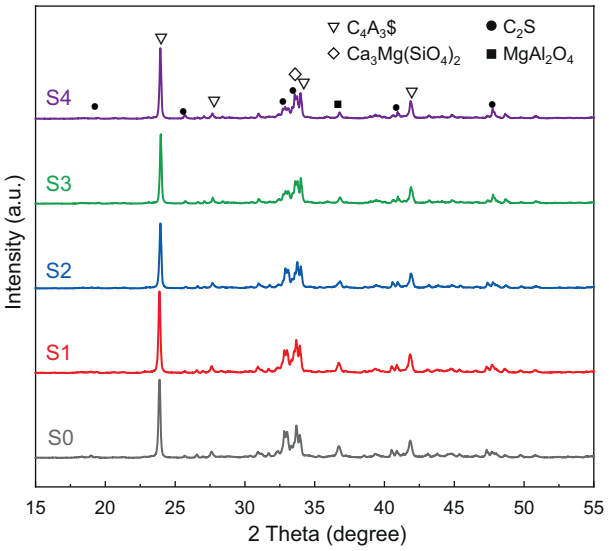

Figure 8. XRD patterns of clinker with different amounts of SO_3.

Figure 8 shows that with the increase in the SO_3 additions, the diffraction peak intensity of $C_4A_3\$$ appears to strengthen and then weaken. This indicates that the SO_3 additions can increase the $C_4A_3\$$ content in the clinker. It is also found that the peak intensity of C_2S and $MgAl_2O_4$ decreases with the increase in the SO_3 additions. Moreover, the C_2S can fix the MgO to produce $Ca_3Mg(SiO_4)_2$.

CONCLUSION

- Dolomite ($CaMg(CO_3)_2$) in high Mg limestone could be decomposed at high temperatures and, thus, release MgO.
- The appropriate firing temperature range of the SWB$C clinker is 1300 °C, which is about 150 °C lower than that of the conventional silicate cement clinker. The main mineral phases of the SWB$C clinker are C_2S, $C_4A_3\$$, $MgAl_2O_4$, and calcium yellow feldspar. Excessive MgO is fixed to produces the stable inertia mineral $MgAl_2O_4$.
- The peak intensity of $MgAl_2O_4$ increased significantly with the extension of the holding time. However, an overly long holding time decreases the amount of $C_4A_3\$$. The *f*-CaO content decreases significantly with the increase in the holding time. The appropriate holding time interval for preparing the clinker was in the range of 60 min ~ 90 min.
- The peak intensity of $C_4A_3\$$ and $MgAl_2O_4$ in the clinker increases significantly as the MgO additions increase, and the over-doped MgO can react with C_2S to form $Ca_3Mg(SiO_4)_2$. SO_3 over-mixing can compensate for the loss of $C_4A_3\$$. The intensity of C_2S and $MgAl_2O_4$ peaks decrease with the increase in the SO_3 additions.

Acknowledgements

This work was supported by the National Key Research and Development Plan of China (No. 2021 YFB3802002), Natural Science Foundations of China (52072149), Natural Science Foundations of China-Shandong Joint Fund (U22A20126).

REFERENCES

1. Gao Y., Li Z., Zhang J., Zhang Q., Wang Y. (2020): Synergistic use of industrial solid wastes to prepare belite-rich sulphoaluminate cement and its feasibility use in repairing materials. *Construction and Building Materials*, *264*, 120201. doi: 10.1016/j.conbuildmat.2020.12020
2. Ban J., Sun K., Yao J., Sunahara G., Hudson-Edwards K., Jordan, G.,et al. (2022): Advances in the use of recycled non-ferrous slag as a resource for non-ferrous metal mine site remediation. *Environmental Research*, *213*, 113533. doi: 10.1016/j.envres.2022.113533
3. Munive G. T., Encinas M. A., Salazar Campoy M. M., Álvarez V. E., Vazquez V. M., Choque D. C. (2020): Leaching Gold and silver with an alternative system: Glycine and thiosulfate from mineral tailings. *Jom*, *72*, 918-924. doi: 10.1007/S11837-019-03652-Z
4. Liu W., Yang J., Xiao B. (2009): Application of Bayer red mud for iron recovery and building material production from alumosilicate residues. *Journal of Hazardous Materials*, *161*(1), 474-478. doi: 10.1016/j.jhazmat.2008.03.122
5. Yu J., Li Y., Lv Y., Han Y., Gao P. (2022): Recovery of iron from high-iron red mud using suspension magnetization roasting and magnetic separation. *Minerals Engineering*, *178*, 107394. doi: 10.1016/j.mineng.2022.107394
6. Li J., Yilmaz E., Cao S. (2021): Influence of industrial solid waste as filling material on mechanical and microstructural characteristics of cementitious backfills. *Construction and Building Materials*, *299*, 124288. doi: 10.1016/j.conbuildmat.2021.124288
7. Huang Y., Wang L., Wu T., Liu W., Tang Q. (2023): Mechanical properties and heavy metal leaching behaviors of municipal solid waste incineration bottom ash as road embankment fillings. *Journal of Cleaner Production*, *394*, 136355.doi: 10.1016/j.jclepro.2023.136355
8. Tang Y., Zhao L., Li B., Chen W. (2022): Controlling the soundness of Portland cement clinker synthesized with solid wastes based on phase transition of $MgNiO_2$. *Cement and Concrete Research*, *157*, 106832. doi: 10.1016/j.cemconres.2022.106832
9. Shen Y., Liu S., Wang Y., Shen P., Xuan D., Guan X., Shi C. (2022): Hydration-hardening properties of low-clinker composite cement incorporating carbonated waste sintering red mud and metakaolin. *Construction and Building Materials*, *354*, 129171. doi: 10.1016/j.conbuildmat.2022.129171
10. Clavier K. A., Paris J. M., Ferraro C. C., Bueno E. T., Tibbetts C. M., Townsend T. G. (2021): Washed waste incineration bottom ash as a raw ingredient in cement production: Implications for lab-scale clinker behavior. *Resources, Conservation and Recycling*, *169*, 105513. doi: 10.1016/j.resconrec.2021.105513
11. Boháč M., Kubátová D., Kotlánová M. K., Khongová I., Zezulová A., Novotný R., et al. (2022): The role of Li_2O, MgO and CuO on SO_3 activated clinkers. *Cement and Concrete Research*, *152*, 106672. doi: 10.1016/j.cemconres.2021.106672
12. Liu G. Q., Yang Q. X., Jiang L., Xue P., Zhang X. L., Han F. L. (2017): Sintering characteristics of BCSAF cement clinker with added wastes from production of manganese and magnesium metals. *Advances in Cement Research*, *29*(6), 227-235. doi: 10.1680/jadcr.16.00035
13. Mo L., Deng M., Tang M., Al-Tabbaa A. (2014): MgO expansive cement and concrete in China: Past, present and future. *Cement and Concrete Research*, *57*, 1-12. doi: 10.1016/j.cemconres.2013.12.007
14. Song Q., Su J., Nie J., Li H., Hu Y., Chen Y., et al. (2021): The occurrence of MgO and its influence on properties of clinker and cement: A review. *Construction and Building Materials*, *293*, 1234. doi: 10.1016/j.conbuildmat.2021.123494
15. Cuesta A., Ayuela A., Aranda M. A. (2021): Belite cements and their activation. *Cement and Concrete Research*, *140*, 106319. doi: 10.1016/j.cemconres.2020.106319.
16. Miller S. A., Myers R. J. (2019): Environmental impacts of alternative cement binders. *Environmental Science & Technology*, *54*(2), 677-686. doi: 10.1021/acs.est.9B05550
17. Glasser F. P., Zhang L. (2001): High-performance cement matrices based on calcium sulfoaluminate-belite compositions. *Cement and Concrete Research*, *31*(12), 1881-1886. doi: 10.1016/S0008-8846(01)00649-4
18. Wang X., Guo M. Z., Yue G., Li Q., Ling T. C. (2022): Synthesis of high belite sulfoaluminate cement with high volume of mixed solid wastes. *Cement and Concrete Research*, *158*, 106845. doi: 10.1016/j.cemconres.2022.106845
19. Shen Y., Qian J., Huang Y., Yang D. (2015): Synthesis of belite sulfoaluminate-ternesite cements with phosphogypsum. *Cement and Concrete Composites*, *63*, 67-75. doi: 10.1016/j.cemconcomp.2015.09.003
20. Xue P., Xu A., He D., Yang Q., Liu G., Engström F., Björkman B. (2016): Research on the sintering process and characteristics of belite sulphoaluminate cement produced by BOF slag. *Construction and Building Materials*, *122*, 567-576. doi: 10.1016/j.conbuildmat.2016.06.098
21. Gallardo M., Almanza J. M., Cortés D. A., Escobedo J. C., Escalante-García J. I. (2014): Synthesis and mechanical properties of a calcium sulphoaluminate cement made of industrial wastes. *Materiales de Construcción*, *64*(315), e023. doi: 10.3989/mc.2014.04513
22. Yan J., Wu F., Li S., Yuan J., Huang Y., Wang S., et al. (2022): Mechanical and chloride ions solidification performance of C_4A_3 ($, P) mineral as promising marine engineering material. *Construction and Building Materials*, *323*, 126553. doi: 10.1016/j.conbuildmat.2022.126553
23. van Gog H. (2021): First-principles study of dehydration interfaces between diaspore and corundum, gibbsite and boehmite, and boehmite and γ-Al_2O_3: Energetic stability, interface charge effects, and dehydration defects. *Applied Surface Science*, *541*, 148501. doi: 10.1016/j.apsusc.2020.148501
24. Yan Z. Q., Wang Z. A., Wang X. F., Hao L. I. U., Qiu J. R. (2015): Kinetic model for calcium sulfate decomposition at high temperature. *Transactions of nonferrous metals society of China*, *25*(10), 3490-3497. doi: 10.1016/S1003-6326(15)63986-3
25. Li R., Zhang J., He W., Nie D., Zhang Y. (2023): Preparation of belite-sulfoaluminate cement with phosphate-rock acid-insoluble residue: Modification and influence of impurity

ions on cement properties. *Construction and Building Materials*, *365*, 130077. doi: 10.1016/j.conbuildmat.2022.130077

26. Winnefeld F., Martin L. H., Müller C. J., Lothenbach B. (2017): Using gypsum to control hydration kinetics of CSA cements. *Construction and Building Materials*, *155*, 154-163. doi: 10.1016/j.conbuildmat.2017.07.217
27. Shen Y., Qian J., Chai J., Fan Y. (2014): Calcium sulphoaluminate cements made with phosphogypsum: Production issues and material properties. *Cement and Concrete Composites*, *48*, 67-74. doi: 10.1016/j.cemconcomp.2014.01.009
28. Li H., Agrawal D. K., Cheng J., Silsbee M. R. (2001): Microwave sintering of sulphoaluminate cement with utility wastes. *Cement and Concrete Research*, *31*(9), 1257-1261. doi: 10.1016/S0008-8846(01)00579-8
29. Singh M., Kapur P. C. (2008): Preparation of calcium sulphoaluminate cement using fertiliser plant wastes. *Journal of Hazardous Materials*, *157*(1), 106-113. doi: 10.1016/j.jhazmat.2007.12.117
30. Fu X., Yang C., Liu Z., Tao W., Hou W., Wu X. (2003): Studies on effects of activators on properties and mechanism of hydration of sulphoaluminate cement. *Cement and Concrete Research*, *33*(3), 317-324. doi: 10.1016/S0008-8846(02)00954-7